Improved deflection calculation methods for traffic speed deflectometers for asphalt pavement condition assessments

Tong, Xiaoying; Chen, Zhang; Cheng, Huailei; Sun, Lijun; Li, Yi; Min, Xuefeng; Jin, Fengcheng

DOI
10.1080/10298436.2025.2498080

Publication date
2025

Document Version
Final published version

Published in
International Journal of Pavement Engineering

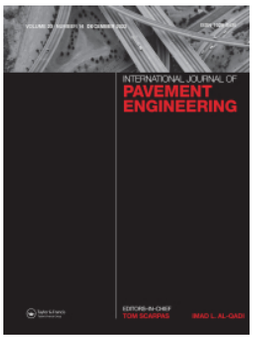

International Journal of Pavement Engineering

ISSN: (Print) (Online) Journal homepage: www.tandfonline.com/journals/gpav20

Improved deflection calculation methods for traffic speed deflectometers for asphalt pavement condition assessments

Xiaoying Tong, Zhang Chen, Huailei Cheng, Lijun Sun, Yi Li, Xuefeng Min & Fengcheng Jin

To cite this article: Xiaoying Tong, Zhang Chen, Huailei Cheng, Lijun Sun, Yi Li, Xuefeng Min & Fengcheng Jin (2025) Improved deflection calculation methods for traffic speed deflectometers for asphalt pavement condition assessments, International Journal of Pavement Engineering, 26:1, 2498080, DOI: 10.1080/10298436.2025.2498080

To link to this article: https://doi.org/10.1080/10298436.2025.2498080

Published online: 29 Apr 2025.

INTERNATIONAL JOURNAL OF PAVEMENT ENGINEERING
2025, VOL. 26, NO. 1, 2498080
https://doi.org/10.1080/10298436.2025.2498080

Improved deflection calculation methods for traffic speed deflectometers for asphalt pavement condition assessments

Xiaoying Tong[a], Zhang Chen[a], Huailei Cheng[a], Lijun Sun[a], Yi Li[b], Xuefeng Min[c] and Fengcheng Jin[c]

[a]The Key Laboratory of Road and Traffic Engineering, Ministry of Education, Tongji University, Shanghai, People's Republic of China; [b]Department of Engineering Structures, Faculty of Civil Engineering and Geosciences, Delft University of Technology, Delft, Netherlands; [c]Hebei Expressway Jingxiong Management Center, Zhangjiakou, People's Republic of China

ABSTRACT

The Traffic Speed Deflectometer (TSD) is increasingly utilised as a nondestructive tool for measuring continuous deflections in asphalt pavements. These deflections are calculated from real-time measurements of deformation velocities recorded using the device's laser vibrometer, combined with the vehicle's travelling speed. However, existing methods for calculating TSD deflections are limited by accuracy and computational efficiency constraints. To address these issues, an improved deflection calculation method was developed. First, finite element (FE) simulations were performed to clarify the deflection slope distribution characteristics of typical flexible and semi-rigid pavements under various conditions. Various fitting curves were then applied to the deflection slope data to identify the most suitable models, and an improved curve area integration method was employed to calculate the corresponding deflection values. Additionally, the impact of different subgrade moduli on the far-end deflection basin of semi-rigid pavements was analyzed, allowing for the determination of the zero-response position of the deflection slope, leding to a proposed correction method for TSD measurements. Finally, the improved deflection calculation method was validated through comparative error analysis with TSD-measured values and FE model results, demonstrating its accuracy and reliability. The findings are expected to support more precise TSD deflection basin determination, improving pavement condition assessment.

ARTICLE HISTORY
Received 22 October 2024
Accepted 21 April 2025

KEYWORDS
Asphalt pavement; TSD; deflection slope; finite element; curve area integration; assessment of pavement conditions

1. Introduction

Deflection plays a crucial role in assessing pavement structural performance and serves as a key reference for designing asphalt pavements and ensuring construction quality (Lee *et al.* 2016, Jia *et al.* 2021, Hu *et al.* 2022). Over the past two decades, non-destructive high-speed laser deflection detection technologies, including the Traffic Speed Deflectometer (TSD) – where 'TSD' in this paper refers broadly to Doppler-laser-based rolling deflection systems rather than a specific commercial product – have been developed and refined. It can continuously and in real-time collect pavement deformation data without interfering with traffic. Attracted by these advantages, it has been increasingly used by various organisations to evaluate the structural load-bearing capacity of in-service asphalt pavements (Manoharan *et al.* 2020, Fan *et al.* 2022, Huang *et al.* 2022, Sun *et al.* 2023, Zhang *et al.* 2023).

Based on the measurement principle, high-speed laser deflectometers are categorised into two types: The first type is distance measurement-based methods, which operate by using laser sensors to measure the vertical displacement of the pavement surface as the device moves along the pavement. Examples of this type include the Rolling Wheel Deflectometer (RWD) (Steele *et al.* 2019, 2020), the Road Deflection Tester (RDT) (Andren and Lenngren 2000), the Rolling Dynamic Deflectometer (RDD) (Nam 2011), and the Ramboll Raptor (Madsen and Pedersen 2022), which combines laser sensors with triangulation and a modified Harr's algorithm for high-precision deflection measurements. The second type is deformation velocity measurement-based methods. These devices measure the deformation velocity of the pavement, combined with the vehicle's travelling speed, which can be used to indirectly calculate pavement deflections, such as the TSD, manufactured by Greenwood Engineering and ARRB Systems (Graczyk *et al.* 2014, Březina *et al.* 2017, Greenwood Engineering 2022).

Due to the fact that deformation velocity of TSD is measured rather than direct displacement, converting this velocity data into accurate deflection values requires thorough analysis and calibration. Currently, two primary methods are employed for this conversion: the elastic foundation beam theory and the multi-layer viscoelastic analytical approach. The elastic foundation beam theory simplifies the pavement as an infinitely long beam on an elastic foundation to calculate the deflection curve. This method offers a simple computational model and ease of implementation, but it fails to reflect actual conditions by ignoring the viscoelastic and nonlinear properties of pavement materials (Krarup *et al.* 2006, Rasmussen *et al.* 2008). In contrast, the multilayer analytical solution incorporates viscoelastic theory to account for the time-dependent behaviour of pavement materials. This approach,

CONTACT Zhang Chen czy1620@263.net; Huailei Cheng chl6218@tongji.edu.cn

combined with finite element modelling or other advanced numerical methods, ensures a comprehensive analysis of both linear and nonlinear material behaviours under dynamic loading conditions, providing a more accurate representation of the complex interactions within pavement structures. For example, Pedersen developed viscoelastic models of pavement deflections specifically for TSD, using continuum mechanics to simulate the behaviour of multilayer asphalt pavement structures under moving loads (Pedersen 2013). Graczyk *et al.* proposed an analytical solution for pavement deflections using the Euler-Bernoulli beam theory supported by a viscoelastic asphalt layer and an elastic subgrade, converting the load into a constant-speed moving concentrated force for simulation analysis (Graczyk *et al.* 2014). Deng focused on the three-dimensional numerical simulation of pavement deflection basins under moving loads, employing finite element (FE) analysis to explore the viscoelastic behaviour of pavement materials and the dynamic effects of loads, and proposed using Gumbel probability density functions to fit the asymmetric deflection basins observed in TSD measurements (Deng 2017). The multilayer viscoelastic analytical solution can more accurately calculate the deflection response under complex pavement conditions by considering the interaction between different layers and the viscoelasticity of the asphalt layers. However, this method is computationally complex, requires extensive input parameters, and is challenging to apply to rapid road detection and real-time data processing. Consequently, developing more accurate and practical calculation methods has become a key focus of current research.

To avoid the complexity of theoretical assumptions and analytical formulas associated with these methods, the curve area integration method was developed as a practical alternative for deflection calculations. This method involves fitting the measured deflection slope data using the Piecewise Cubic Hermite Interpolating Polynomial (PCHIP) and then integrating the area under the curve (this approach is referred to as the AUTC-PCHIP method). The integration starts from the reference sensor located at 3,500 mm from the load centre (i.e. S3500), to obtain the deflection value. This approach effectively addresses the issue of unreliable deflection value calculations at locations far from the load centre and has been widely adopted in the industry (Muller and Roberts 2013, Zofka *et al.* 2014, Xiao *et al.* 2021, Shen and Wang 2023). However, this method also has some drawbacks. Firstly, the PCHIP heavily relies on readings from selected sensors. If the sensor readings do not accurately reflect the actual changes in deflection slope – for instance, assuming the maximum deflection slope readings at sensors S100 or S200 while the theoretical maximum deflection slope position deviates from these locations – errors in calculation will occur. Secondly, the deflection slope is influenced by various complex factors, such as pavement structure, material properties, and environmental conditions. The PCHIP may not fully capture the effects of these factors (Cao *et al.* 2019, Cheng *et al.* 2019, 2020, 2021, Steiner *et al.* 2016). Additionally, the assumption regarding the integration position has significant flaws. The current AUTC-PCHIP method assumes a zero-response position for the deflection slope at sensor S3500, which is relatively reasonable for flexible asphalt pavement. However, its applicability to semi-rigid pavements lacks sufficient research support. Therefore, the existing curve area integration method still requires further research and improvement, particularly regarding its reliance on PCHIP and the limitations inherent in the integration position assumption.

This study aims to develop an improved deflection calculation method using curve area integration, enabling more accurate and rapid calculation of deflection basins under TSD loads. This improved deflection calculation method is referred to as the Area Under the Curve – Composite Polynomial Model (AUTC-CPM), which emphasises its foundation on curve area integration and the use of composite polynomial fitting techniques for accurate deflection basin calculations. Firstly, the finite element (FE) method was employed to establish a mechanical model of viscoelastic asphalt pavement structures. This model was utilised to evaluate the influence of various conditions on TSD theoretical deflection and deflection slope, thereby clarifying the theoretical deflection slope distribution characteristics of typical asphalt pavement structures under TSD loads. Secondly, appropriate deflection slope curve forms were selected, the theoretical deflection slope data calculated by the FE method under different conditions were fitted, and an improved curve area integration method was employed to calculate the corresponding deflection values. Subsequently, take semi-rigid pavement for example, the actual range of load propagation was determined through the FE model, and the position where the theoretical zero-response position of deflection slope was identified. This approach established a more scientifically grounded integration reference baseline for semi-rigid pavement structures and facilitated the correction of measured values. Finally, the deflection values obtained by the AUTC-CPM method were compared with the measured values and those calculated by the FE method to evaluate its effectiveness and accuracy.

2. TSD tests and deflection calculation framework

To ensure accurate pavement deflection assessments, the configuration of the TSD vehicle and sensors, the process of data collection and preprocessing, and the methodology for calculating deflections from TSD-measured data are systematically presented.

2.1. TSD vehicle and sensor configuration

The deflection detection equipment used in this study is a TSD device, designated as model 11 (RAB Shanghai, China), produced by the Greenwood Engineering Company (as shown in Figure 1(a)). The TSD system comprises several key components: a carrier vehicle, a Doppler laser vibrometer system (which includes speed measurement system), a detection control system, a temperature control system, and a data processing system. The core component, the Doppler laser vibrometer, is positioned at the centre of the vehicle's right rear wheel gap and is equipped with seven laser sensors along the driving direction. The Doppler lasers operate based on the Doppler effect, where the frequency of the reflected laser signal shifts proportionally to the relative

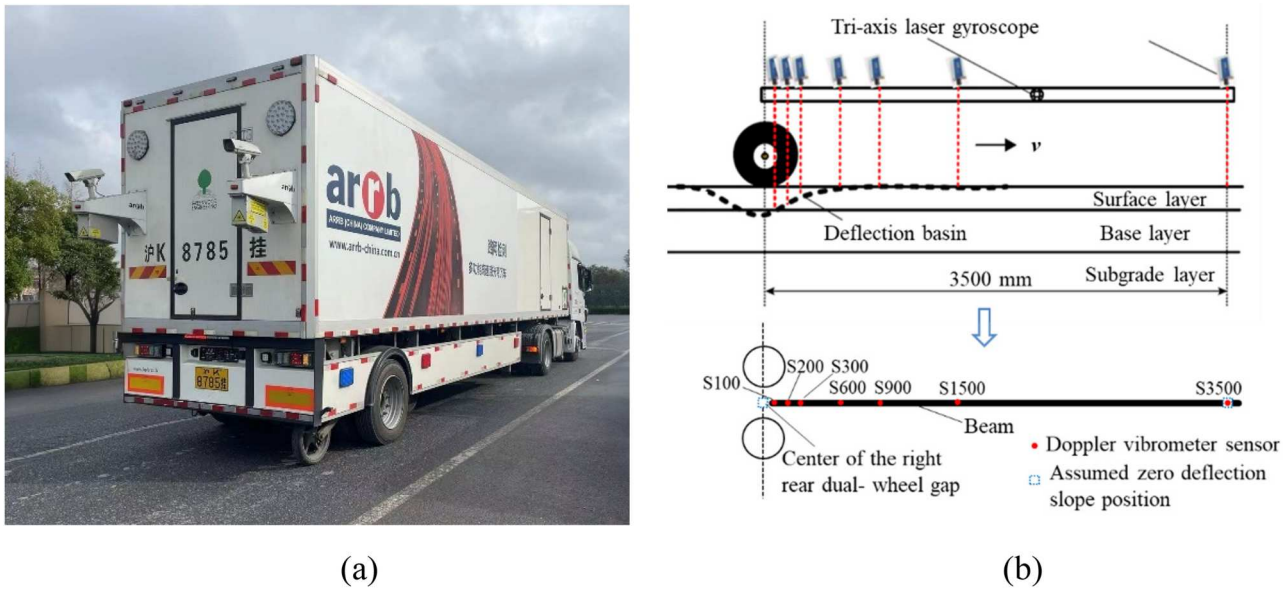

Figure 1. Composition of the TSD11 vehicle: (a) appearance of the TSD11 vehicle; and (b) schematic of Doppler sensor positions relative to the rear wheel centre.

motion of the pavement surface. This enables the TSD to precisely measure pavement deformation velocity. By combining this velocity with the vehicle's travelling speed, the TSD calculates the deflection slope at specific offsets near the moving load.

The carrier vehicle of TSD has a total length of 8.6 m, with a rear axle load of 100 kN and a tire inflation pressure of 0.7 MPa. The Doppler sensors are positioned at offsets of 100, 200 mm, 300, 600, 900 m, 1,500 mm, and 3,500 mm from the rear wheel centre, corresponding to the sensors labelled as S100, S200, S300, S600, S900, S1500, and S3500, respectively (as shown in Figure 1(b)). Among them, the sensor of S3500 serves as the reference sensor, which is assumed to remain unaffected by the applied load, with its vertical pavement deflection velocity presumed to be zero (Duschlbauer and Lee 2021, Beizaei 2023).

The data processing system of TSD outputs key parameters that encompass vehicle dynamics (e.g. driving speed, GPS positioning), environmental conditions (e.g. pavement and air temperature), sensor data (e.g. laser measurements, strain gauges), and pavement deflection characteristics (e.g. vertical deflection velocity, deflection slope). These parameters collectively provide comprehensive insights into pavement structural performance and facilitate effective road condition assessments.

2.2. TSD test and data collection

2.2.1. Selection of TSD test section

To ensure that the TSD test provides reliable data for evaluating pavement structure performance, the total length of the test section was selected as 1,500 m (at least 1,000 m). The functions of different portions of the test section are as follows: 1). The initial 300 m acceleration zone to reach the specified test speed; 2). The 500 m to 1,000 m data collection zone where the TSD operated at a constant speed; 3). The final 200 m deceleration zone to safely slow down (see Figure 2).

The test section consists of a semi-rigid asphalt pavement. The specific composition is as follows: the thickness of surface layer is 12 cm, consists of two dense-graded asphalt concrete layers: a 4 cm upper layer of AC-13, featuring a nominal maximum aggregate size of 13 mm, and an 8 cm lower layer of AC-25, with a nominal maximum aggregate size of 25 mm. The base layer is constructed with cement-stabilised crushed stone with a thickness of 36 cm, and the subgrade layer is constructed with graded crushed stone with a thickness of 15 cm.

2.2.2. TSD data collection and preprocessing

The TSD testing method adheres to relevant standards, and Doppler sensor calibration needs to be completed prior to testing (Ministry of Transport 2017, Austroads 2016, FHWA 2016). At the test's outset, all systems should be activated and verified to ensure that the computer, software collection, computation, and warning lights are functioning correctly. The specific testing steps are as follows:

1) Position marking: mark the starting and ending positions of the test section, and the start and end of the detection area (see Figure 3(a) and (b)).
2) Equipment calibration: calibrate the measurement equipment before conducting the TSD test, to ensure accurate vehicle positioning and sensor alignment.
3) Track assignment: on the test section, mark clear measurement tracks along the wheel path parallel to the lane line and mark detection positions every 10 metres with paint.
4) Data collection: position the centre of the TSD's right rear wheel at the test section's starting point. Turn on the data collection system before starting the vehicle. Accelerate in the acceleration area and maintain a constant speed range from 10 km/h to 50 km/h in intervals of 10 km/h in the detection area, ensuring the laser aligns as closely as possible with the marked measurement line until data collection stops after passing the end position (see Figure 3(c)). For each testing, at least three repeated tests were

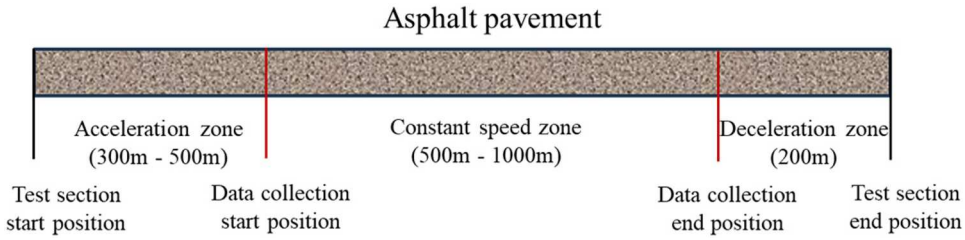

Figure 2. Schematic diagram of the test section.

performed to calculate the average value ensuring accuracy and reliability. Finally, statistical methods were used to eliminate outliers in the TSD test data.

2.3. Framework for the calculation of TSD deflections

Figure 4 illustrates the developed framework for accurately calculating TSD deflection values. The framework includes the following key steps:

1) Establish a mechanical model of typical asphalt pavement structures (flexible and semi-rigid pavements) using the FE method. Consider the viscoelastic properties of the asphalt layer to simulate pavement deformation under rolling loads from the TSD. The simulation conditions include various travelling speeds (v), temperatures (T), base layer moduli (E_b), subgrade moduli (E_s), and pavement thicknesses (H) (represents the combined thickness of the surface and base layers, excluding the subgrade). This comprehensive evaluation assesses the potential impact of these conditions on TSD theoretical deflection and deflection slope.
2) Identify the theoretical deflection slope distribution characteristics of typical asphalt pavement structures under TSD loading. Analyze the deflection slope curve characteristics and extreme values of flexible and semi-rigid pavements under different conditions to provide a basis for subsequent curve fitting and baseline determination.
3) Select an appropriate deflection slope curve form. Fit the deflection slope data by the FE method to the chosen curve, ensuring that the fitting results accurately reflect the overall trend of the theoretical deflection slope.
4) Given the common assumption in TSD deflection calculations that the deflection slope at sensor S3500 is 0 μm/m – reasonable for flexible asphalt pavement structures but requiring further validation for semi-rigid pavement structures – determine the actual range of load propagation through the FE model. Identify the position where the deflection slope is 0 μm/m to establish a more scientific integration reference baseline for semi-rigid pavement structures.
5) Use the selected curve fitting method to integrate and calculate the deflection values at each offset sensor. For pavement structures where the deflection slope at S3500 is not a theoretical zero-response position, adjust the deflection values based on the characteristics of the pavement structure and testing conditions.
6) Analyze the differences between the TSD measured data and FE model values to determine deflection slope discrepancies across offsets from 0 mm to 9,000 mm. For sensors offsets $\leq$ 3,500 mm, utilise the FE value at the 3,500 mm offset as the correction value. For offsets > 3,500 mm, employ the corresponding FE model values as correction factors.

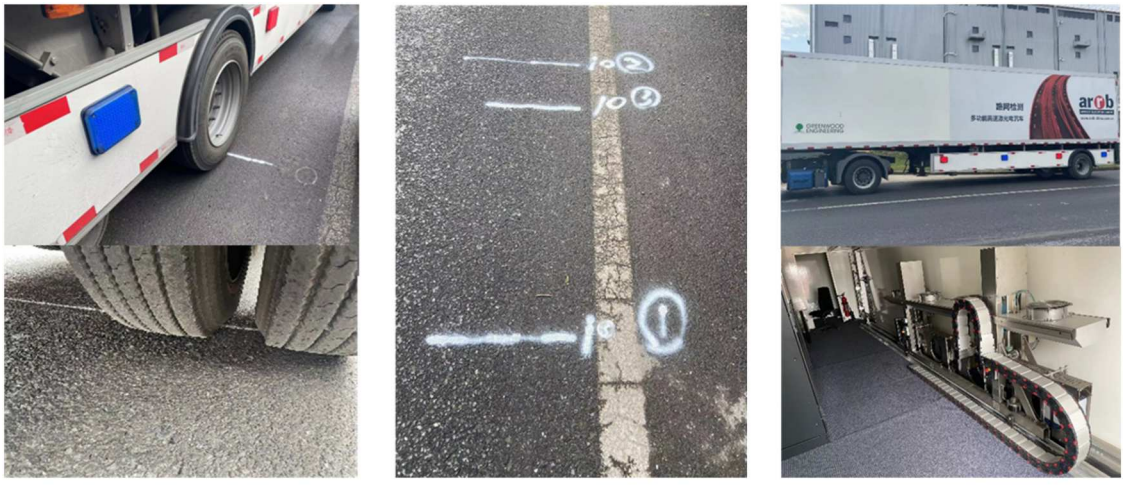

Figure 3. Data collection in the test section: (a) start position marker of the test section; (b) end position marker of the test section; and (c) TSD data collection in the test section.

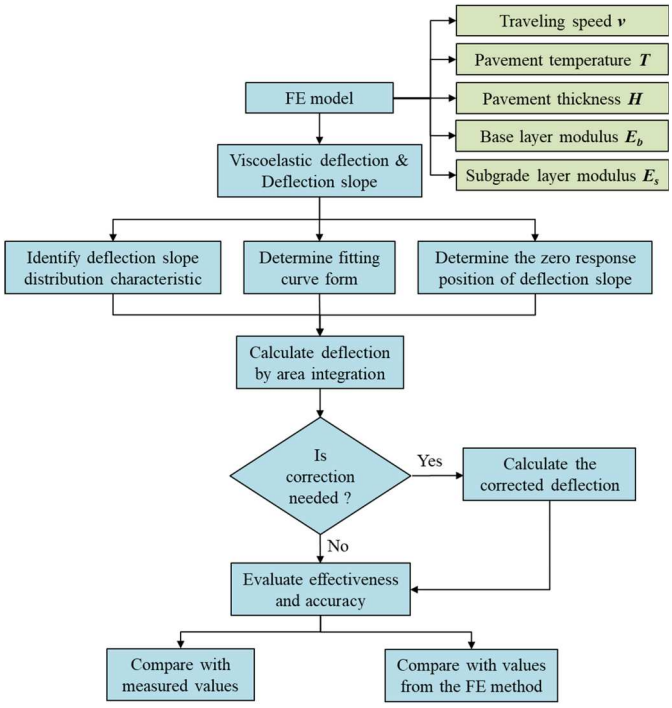

Figure 4. Flowchart of the improved deflection calculation method.

7) Compare the deflection values obtained by the proposed method with measured values and values from the FE method to evaluate the effectiveness and accuracy of the calculation method.

3. Improved curve area integration method for deflection calculation

To improve the accuracy of deflection calculations, the characteristics of deflection and deflection slope distributions are analyzed, a deflection slope fitting method is established, the theoretical zero-response position is defined, and correction strategies for semi-rigid asphalt pavements are proposed based on an improved curve area integration approach.

3.1. Deflection and deflection slope distribution characteristics of typical asphalt pavements

3.1.1. Pavement types

Two typical asphalt pavements were selected for evaluation in this research: a flexible asphalt pavement and a semi-rigid asphalt pavement. The base layer of the flexible pavement consists of graded crushed stone, while the semi-rigid pavement features a base layer of cement-stabilised crushed stone. Both types of pavements have a surface layer of dense-graded asphalt concrete (namely AC-13) and a subgrade of lime-treated soil (see Figure 5(a)). The basic structural parameters of two typical pavements are detailed in Table 1.

3.1.2. Material characterisation

Asphalt mixture exhibits viscoelastic properties, with its modulus varying significantly with temperature and loading conditions (Deng *et al.* 2019, Wu *et al.* 2020, Mabrouk *et al.* 2022). The generalised Maxwell model was applied to characterise the viscoelastic behaviours of the asphalt mixture. The relaxation modulus was derived from dynamic modulus tests at specific temperatures and loading frequencies (Chen *et al.* 2024). Specifically, the dynamic modulus and phase angle data were converted into relaxation modulus values using the Schapery and Park method (Park and Schapery 1999, NCHRP 2004). To obtain the master curve, the relaxation modulus was fitted using a Sigmoid function. Figure 5(b) presents the fitted master curve, and Figure 5(c) shows the fitting results of the generalised Maxwell model (T = 20°C).

Subsequently, the relaxation modulus master curve was fitted to a fifth-order generalised Maxwell model, capturing the viscoelastic behaviour of the asphalt mixture across a wide range of relaxation times. The resulting fitting parameters, including relaxation times and moduli, were then converted into Prony series coefficients required for input into the ABAQUS FE model. These coefficients, summarised in Table 2, enable precise representation of the time-dependent viscoelastic behaviour in the finite element simulations.

3.1.3. FE model

To accurately simulate the behaviours of asphalt pavements under TSD loads, FE models were incorporated, as shown in Figure 5(d). The pavement model in this research was settled to have dimensions of 11 m in length, 7 m in width, and 8 m in height to balance computational efficiency with accuracy (Chen *et al.* 2024). The interfaces between different pavement layers were assumed to be fully bonded (Roussel *et al.* 2019, 2022). The contact area of the wheel load in the model was determined according to the TSD load information. Specifically, the contact area was rectangular with a length of 0.274 m and a width of 0.127 m, while the contact pressure was set to 0.7 MPa. To mitigate boundary effects, infinite elements were applied at the model boundaries. This approach ensures that the simulated domain effectively replicates an unbounded medium, eliminating artificial reflections and enhancing the accuracy of deflection calculations within the region of interest. The boundaries of the FE model were fixed only in the normal direction, while the bottom of the model was fixed in all three directions.

To simulate the moving load of the TSD facility, the DLOAD subroutine was employed in the FE model to shift the contact area of the wheel load with a certain speed. The moving speed of the contact area ranged from 5 km/h to 120 km/h, allowing for the evaluation of the effects of different speeds on TSD deflections. The element type used in the FE model was C3D8I. The analysis algorithm employed in the FE model was dynamic implicit. A fine mesh was applied near the loading area, while a relatively coarse mesh was utilised for regions farther from the loading centre to enhance computational efficiency. The mesh size at the loading centre was set to $0.032\text{m} \times 0.017\text{m} \times 0.011$ m. The accuracy of the dimension and mesh size of the model has been validated in previous research (Chen *et al.* 2024).

The FE model employed in this study represented the linear elastic behaviours of the base and subgrade layers, and the linear viscoelastic behaviour of the asphalt layer, facilitating the dynamic analysis of varying load conditions.

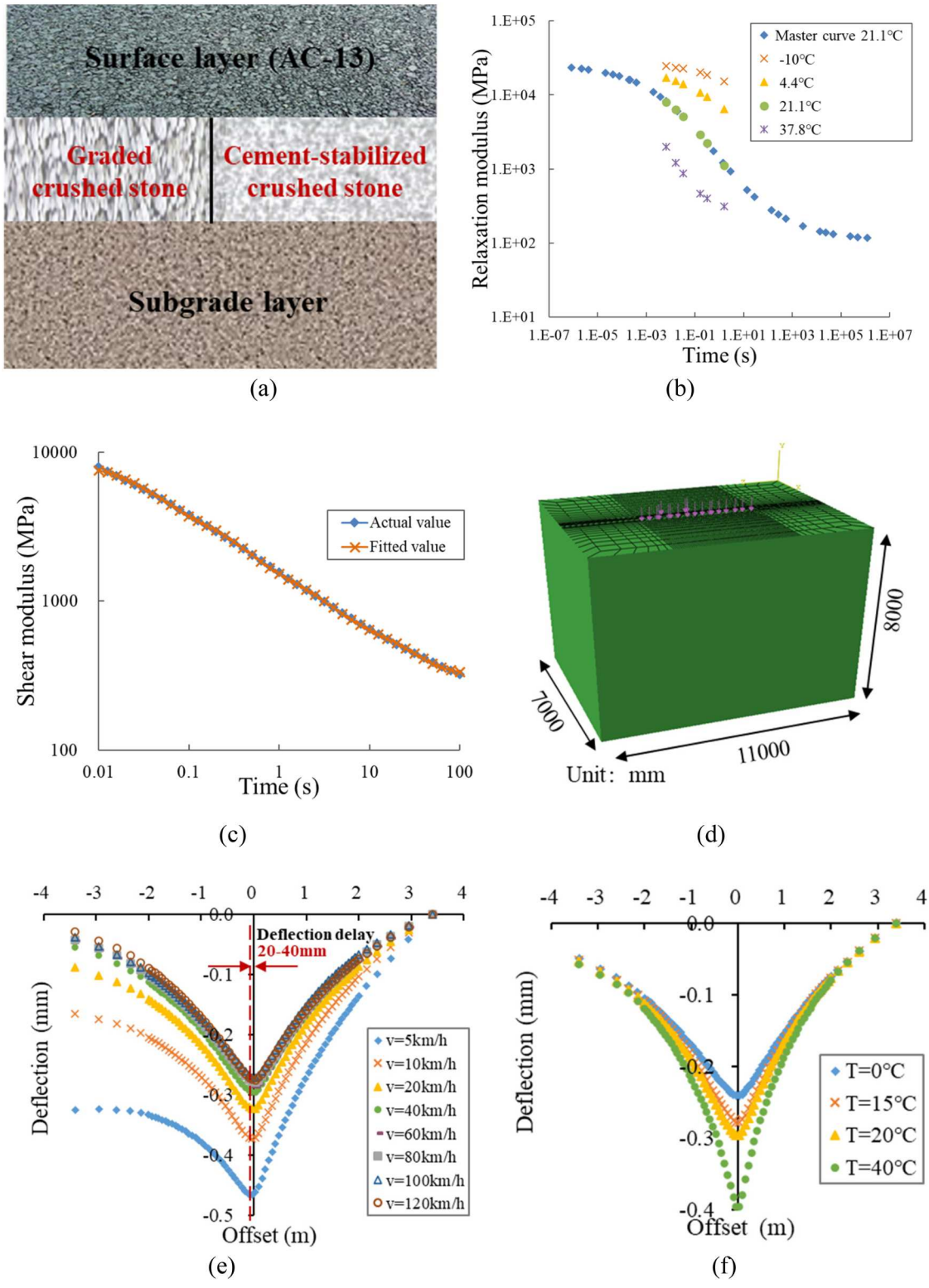

Figure 5. Diagram for the parameters of the FE model for asphalt pavement: (a) diagram of typical pavement; (b) the master curve of relaxation modulus of asphalt pavement; (c) the fitting results of the generalised Maxwell model (T = 20°C); (d) diagrams of FE model; (e) The effect of driving speed on FE deflection; (f) The effect of temperature on FE deflection.

3.1.4. Simulation scenarios

Various conditions were considered to analyze their potential impact on deflection values, including different travelling speeds, temperatures, surface layer thicknesses, base layer thicknesses, base layer moduli, and subgrade moduli. The detailed parameters of the pavement models are shown in Table 3. By using the FE method, various conditions for the two types of typical asphalt pavement were simulated, resulting in a total of 16,000 scenarios for flexible pavements and 22,400 scenarios for semi-rigid pavements.

Table 1. Summary of pavement structures investigated in this research.

Layer	Type	Density (kg/m^3)	Thickness (cm)	Modulus (MPa)	Poisson's ratio
Surface layer	AC-13	2,400	10–50	Dynamic modulus	0.35
Base layer (Flexible)	Graded crushed stone	2,000	30–70	200-1,000	0.35
Base layer (Semi-rigid)	Cement-stabilised gravel	2,200	30–70	5,000-20,000	0.25
Subgrade layer	Lime soil	1,800	-	60–200	0.4

Table 3. The detailed settlements of pavement models.

Scenarios	Unit	Flexible	Semi-rigid
Travelling speed of TSD (v)	km/h	5, 10, 20, 40, 60, 80, 100, and 120	5, 10, 20, 40, 60, 80, 100, and 120
Temperature (T)	℃	0, 15, 20, and 40	0, 15, 20, and 40
Surface layer thickness (H_1)	cm	10, 20, 30, 40, and 50	10, 20, 30, 40, and 50
Base layer Thickness (H_2)	cm	30, 40, 50, 60, and 70	30, 40, 50, 60, and 70
Base layer Modulus (E_b)	MPa	200 - 1,000 (Interval 200)	5,000 - 20,000 (Interval 2,500)
subgrade layer modulus (E_s)	MPa	60, 100, 140,180	60, 100, 140,180
Sum of scenarios	-	16,000	22,400

For this study, a temperature of 20°C, surface layer thickness of 20 cm, base thickness of 40 cm, and base layer modulus of 600 MPa, subgrade modulus of 60 MPa were used as Example 1, the effect of driving speed on flexible deflection as shown in Figure 5 (e). A driving speed of 40 km/h, surface layer thickness of 20 cm, base thickness of 40 cm, and base layer modulus of 600 MPa, subgrade modulus of 60 MPa were used as Example 2, the effect of temperature on flexible deflection as shown in Figure 5 (f). A driving speed of 40 km/h, a temperature of 20°C, a surface layer thickness of 20 cm, a base layer thickness of 40 cm, and a subgrade modulus of 60 MPa were used as Example 3. The deflection slope distribution for two types of asphalt pavement structures under different base moduli, as shown in Figure 6.

Figure 5(e) clearly illustrates that lower vehicle speeds result in a significant increase in maximum deflection, suggesting that lower speeds significantly amplify the pavement's response. Importantly, this effect is exacerbated by the viscoelastic properties of asphalt materials, which cause a delay in the response time of the pavement to reach maximum deflection – a phenomenon referred to as 'deflection delay'. This deflection delay is a critical behaviour of asphalt pavements, reflecting the time-dependent nature of the material. At reduced speeds, the load is applied over a longer duration, allowing the viscoelastic materials more time to deform. This results in a delay in reaching the peak deflection point compared to conditions at higher speeds, where the response is more immediate due to the shorter load application time.

Figure 5(f) shows the impact of temperature on asphalt deflection is distinct across a range from 0°C to 40°C. Higher temperatures lead to deeper deflections as the asphalt material becomes less stiffness and more ductile, allowing it to deform more readily under load. Conversely, as temperatures decrease, the asphalt becomes more rigid, reducing its ability to deform, which consequently decreases the depth of deflections.

Figure 6 presents the theoretical calculation results of deflection slopes for two typical asphalt pavement structures under TSD loads, leading to the following conclusions: 1) Curve characteristics: the deflection slope of flexible asphalt pavement initially decreases, then increases, and finally decreases again across the load application area. In the front area of the applied load (right side of Figure 6), the deflection slope shows one maximum value. Unlike flexible pavements, the deflection slope of semi-rigid asphalt pavements exhibits multiple extremum values, including both maxima and minima in the front load area. Additionally, under the same load conditions, semi-rigid pavements generally exhibit lower deflection slopes than flexible pavements, indicating a close relationship between pavement stiffness and deflection slope. The modulus distribution in semi-rigid pavements is highest in the base layer, followed by the surface layer, and lowest in the subgrade, resulting in smaller but more complex deformations and multiple extremum values. 2) Extremum characteristics: statistical analysis of deformation results under different conditions shows that the maximum value positions for flexible pavements correspond to the TSD sensor range of approximately S200-S450. For semi-rigid pavements, the maximum value positions correspond to the range of S100-S200, and the minimum value positions to S300-S450. The lower modulus and higher elasticity of flexible pavements cause more dispersed stress and deformation, leading to wider sensor range extremum positions. Conversely, the high modulus and low elasticity of semi-rigid pavements cause more concentrated stress and deformation, leading to narrower sensor range extremum positions.

Table 2. The fitting results of the fifth-order Maxwell model for the relaxation modulus.

n	1	2	3	4	5
E_i (MPa)	1709.8	4610.1	2436.7	1030.5	457.2
ρ_i	0.0001	0.0325	0.2909	2.3831	23.1896
E_∞ (MPa)			326.8		
R^2			0.99		

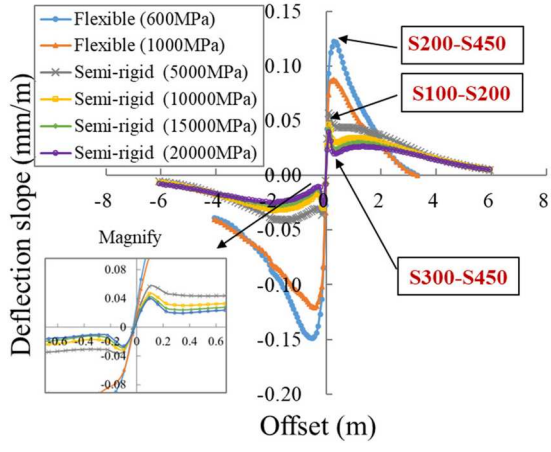

Figure 6. deflection slope distribution of typical pavement.

As shown in Figure 6, the deflection slope of semi-rigid pavements decreases more gradually compared to flexible pavements. This variance is largely attributed to differences in material stiffness and the viscoelastic properties of the asphalt layers. Flexible pavements, with a relatively low modulus and enhanced elasticity, allow for broader distribution of stress and deformation under load, resulting in a more even dissipation of load-induced stresses. In contrast, semi-rigid pavements, due to higher modulus and reduced elasticity, experience localised stress concentrations under load, causing deformation to be transmit less efficiently across the pavement structure.

Overall, the deflection slopes of semi-rigid asphalt pavements typically do not reach 0 μm/m near an offset of 3,500 mm. Therefore, when utilising the TSD to assess asphalt pavements, it is critical to accurately identify the zero-deflection slope location. If the reference sensor offset is not properly adjusted to reflect the actual pavement characteristics, significant errors may arise when converting TSD-measured deflection slopes into actual deflection values. Such inaccuracies may considerably impact the precision of pavement condition assessments, potentially influencing maintenance strategies and design decisions. Given the unique viscoelastic properties and slower deflection response of semi-rigid pavements, subsequent research will primarily focus on addressing the complexities associated with semi-rigid pavements.

3.2. Determining the deflection slope fitting curve

Based on the models described in Section 3.1, the viscoelastic deflections of asphalt under TSD load were calculated and fitted to over one hundred different curve forms. The fitting effectiveness was comprehensively evaluated using the coefficient of determination (R^2) and the root mean square error (*RMSE*).

First, using $R^2 > 0.9$ as a criterion, nine curve forms were initially selected (see Eq. (A.1) – Eq. (A.9) in the Appendix). These nine curve forms were then used to refit the deflection data under all conditions (see Table 3). To further analyze the fitting quality, *RMSE* was used for evaluation, as shown in Equation (1). Finally, the *RMSE* was categorised into several classes: 0%∼2%, 3%∼5%, 5%∼10%, 10%∼15%, 15%∼20%, 20%∼25%, and 25%∼100%, and the cumulative probability for each category was calculated. The distribution of cumulative probability is shown in Figure 7.

$$RMSE = \sqrt{\frac{1}{n}\sum_{k=1}^{n}\left(\frac{w_{cal} - w_{fit}}{w_{fit}}\right)^2}, \tag{1}$$

where, w_{all} represents the theoretical deflection value calculated by the FE method, and w_{fit} represents the fitted deflection value.

As shown in Figure 7, the *RMSE* of the third-order Composite Polynomial Model (CPM) (detailed in Eq. (A.1)), second-order CPM equations (see Eq. (A.2) through (A.4)), and the fifth-order polynomial (see Eq. (A.8)) is mainly concentrated in the range of 0%∼2%, indicating superior fitting results. In contrast, other equations (detailed in Eq. (A.5) through (A.7) and Eq. (A.9)) exhibited poorer fitting performance and

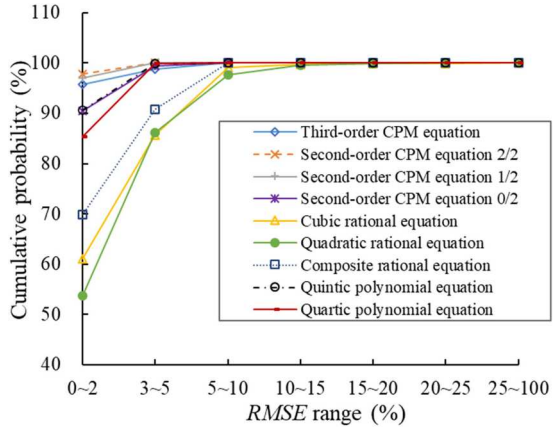

Figure 7. Cumulative probability of *RMSE* for different fitting curves.

were excluded from further analysis. Notably, although the third-order CPM and fifth-order rational function demonstrated high accuracy in fitting theoretical deflection values, their highest derivative order reaches six. Given that the TSD laser sensor system includes only seven sensors, high-order or complex functions can lead to overfitting, particularly when integrating actual measured deflection slope data. To avoid overfitting and simplify computational complexity, this study excluded equations with derivative orders exceeding five (such as Eqs. (A.1) and (A.8)) and those with complex derivative structures (such as Eqs. (A.2) and (A.3)). Ultimately, the second-order CPM 0/2 (see Eq. (A.4)) was selected as the preferred curve type for fitting the deflection basin. The specific forms of the deflection and deflection slope curves are given by Equations (2) and (3).

$$y = \frac{a}{1 + bx + cx^2} \tag{2}$$

$$y' = -\frac{dx + e}{1 + fx + gx^2 + hx^3 + jx^4} \tag{3}$$

In summary, given the complexity of pavement structures, this study applied various curve forms for data fitting based on the FE model results under different conditions. Through the evaluation of R^2 and *RMSE*, the second-order CPM 0/2 equation was identified as the optimal fitting curve for the theoretical deflection slope. This method provides an effective prediction model for deflection slopes, demonstrating improved prediction accuracy under diverse pavement conditions. The adaptability of the CPM 0/2 equation to complex pavement structures ensures more reliable results when applied to real-world road conditions.

3.3. Defining the zero-response position of deflection slope

As discussed in Section 3.1, the deflection slope of asphalt pavement at an offset of 3,500 mm is not the zero-response position (i.e. deflection slope is 0 μm/m), indicating that the reference sensor S3500 of the TSD is still within the theoretical deflection basin during detection. The zero-response position is crucial, as it represents the point beyond which the influence

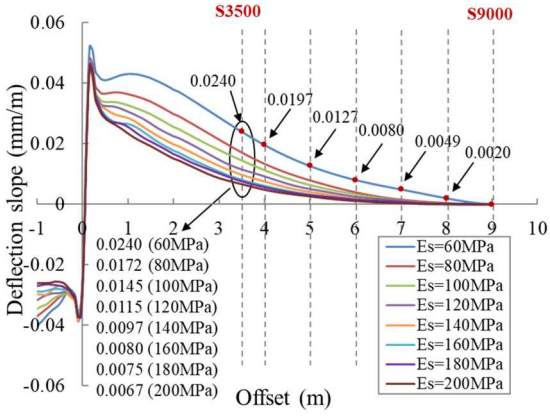

Figure 8. Deflection slope of semi-rigid asphalt pavement under different subgrade moduli.

of the applied load is negligible, and the deflection slope theoretically returns to zero. Accurately identifying this position is essential for establishing a reliable baseline for deflection measurements.

To accurately define the reference positions where the deflection slope is 0 μm/m, it is necessary to clarify the actual range of load propagation on semi-rigid pavements and establish a more scientific reference baseline. Given that the deformation at the far offset of semi-rigid asphalt pavement is significantly influenced by the subgrade modulus E_s (Shi *et al.* 2022, Zhang *et al.* 2024), this study used subgrade resilient moduli E_s ranging from 60 MPa to 200 MPa, with an interval of 20 MPa. The FE method was then used to examine the impact of varying subgrade moduli on the deflection slope at different offsets. The specific results are shown in Figure 8.

The change in deflection slope is represented by the absolute rate of change between adjacent intervals, as shown in Equation (4):

$$R = \frac{|DSi + 1 - DSi|}{(Si + 1 - Si)^2}, \tag{4}$$

where, R represents the absolute rate of change in deflection slope values, i is the index of the deflection sensor, S_i represents the distance of the i – th sensor from the TSD load centre, and DS_i represents the deflection slope value at any offset (i.e. S_i).

Figure 8 shows the theoretical deflection slope curves of semi-rigid pavement structures under different subgrade modulus conditions. It can be observed that at the offset of 3,500 mm, the deflection slope does not drop to 0 μm/m under various subgrade modulus conditions. For instance, when the subgrade modulus is set to 60, 100, 140, and 200 MPa, the corresponding deflection slopes at S3500 are 24, 14.5, 9.7, and 6.7 μm/m, respectively. These results indicate that as the subgrade modulus decreases, the deflection slope of semi-rigid pavements increases, resulting in more significant pavement deformation and a larger influence range during TSD testing. Therefore, when using TSD to measure the deformation of semi-rigid asphalt pavement structures, it is necessary to extend the TSD beam length according to the actual deflection basin range to ensure the reference sensor is positioned outside the deflection basin.

To determine the offset where the theoretical deflection slope is 0 μm/m, this study selected a subgrade modulus of 60 MPa and positioned the reference sensor at different offsets from the loading centre: specifically at 3,500 mm, 4,000 mm, 5,000 mm, 6,000 mm, 7,000 mm, 8,000 mm, and 9,000 mm. Using the deflection slope at 3,500 mm as a baseline, the absolute rates of change at other offsets were calculated to be 17.2, 7.0, 4.6, 3.1, 2.9, and 2.0 μm/m², respectively. The results show that as the offset increases, the rate of change in the deflection slope gradually decreases and stabilises at an offset of 9,000 mm. This trend indicates that at a 9,000 mm offset, the rate of change in the deflection slope becomes stable, and the deflection response is no longer affected by the load beyond this distance, achieving a steady state. Therefore, it is necessary to position the reference sensor at least 9,000 mm from the load centre to ensure the accuracy of TSD deflection calculations and the reliability of the test data.

3.4. Corrections of TSD deflection for semi-rigid asphalt pavements

TSD deflection slopes of were corrected by taking semi-rigid pavement structures as an example. Based on the findings from Section 3.3, accurate measurement of surface deformation in semi-rigid pavement structures using TSD necessitates precise sensor positioning. Ideally, to accurately capture the theoretical zero deflection slope, the reference sensor should be positioned at 9,000 mm from the load centre. However, due to practical constraints such as vehicle axles of the TSD, the deflection slopes measured on the test road are still based on the readings corrected by the reference sensor S3500.. This position, while not ideal for capturing the zero slope, has been validated for practical use and allows for consistent, albeit adjusted, measurements, these adjustments specifically involve subtracting the deflection values measured at the 3.5-meter sensor from the overall deflection velocities to accurately depict the corresponding deflection slopes. To address the discrepancies caused by this non-ideal sensor placement of semi-rigid pavement and enhance measurement accuracy, correction factors derived from FE models are applied to the data collected from the seven sensors on the TSD vehicle. These correction factors are meticulously calculated to adjust for the variances introduced by the sensor's proximity to the load centre, ensuring that the measurements reflect accurate deflection profiles of semi-rigid pavements.

Specifically, the FE model results are used to determine the theoretical deflection slopes at various offsets, and these values are used to adjust the TSD measurements. This method would be validated by comparing the corrected deflection values with those obtained from the FE model, confirming the accuracy of the corrections and the reliability of the TSD measurements under these conditions. Therefore, this study combined with TSD measured data from Section 2.1.3, and proposed a correction method based on the values from the FE model, with the following specific steps:

1) Use the FE method to accurately simulate the model and analyze the distribution of deflection slopes in semi-rigid

pavements. The simulation should consider factors such as the actual pavement structure, material properties, loading speed, temperature, load size, and its distribution.

2) From the FE results, determine the new reference sensor offset where the theoretical deflection slope is 0 μm/m. In this study, the reference position of semi-rigid pavement is determined to be 9,000 mm from the centre of the rear axle gap.
3) Analyze the differences between the TSD measured data and the FE model values to determine the deflection slope differences at varying offsets from 0 mm to 9,000 mm. For sensor offsets ≤ 3,500 mm, use the fixed value from the FE model at the offset of 3,500 mm as the correction value. For offsets > 3,500 mm, use the values from the FE model as the correction value. The formula for calculating the corrected deflection slope values is given in Equation (5).

$$DScorrected = \begin{cases} DSmeasured + DSFE, S3500 & \text{if } Si \geq 3500\text{mm} \\ DSmeasured + DSFE, Si & \text{if } Si > 3500\text{mm}, \end{cases} \quad (5)$$

where, $DS_{corrected}$ is the corrected deflection slope, $DS_{measured}$ is the TSD measured deflection slope, $DSFE, S3500$is the deflection slope from the FE method at the S3500 offset, and$DSFE, Si$is the deflection slope from the FE method at the S_i offset.

4) Set the zero-position of the deflection slope at 9,000 mm from the load centre. Then, use the AUTC-CPM to obtain the fitted deflection curve, and compare it with the FE values and corrected deflection values.
5) Verify the correction results by comparing the deflection values calculated using the FE method to assess the accuracy of the corrections.

As shown in Figure 9(a), correcting the measured deflection slopes of the semi-rigid pavement structure accurately reflects actual conditions, thereby ensuring the accuracy and practicality of TSD data. The specific method is as follows: For sensor offsets ≤ 3,500 mm, uniformly add the theoretical values calculated by the FE method at the offset of 3,500 mm (e.g. 31.273). For offsets > 3,500 mm, directly add the FE model values at each offset.

To evaluate the accuracy of the corrected deflection values, as shown in Figure 9(b), the deflection values derived from the AUTC-CPM method, the original TSD measured deflection values, and the deflection values calculated using the FE model were compared. The comparison reveals that: 1) The original TSD measured deflection values deviate significantly from the theoretical deflection values predicted by the FE model, indicating substantial measurement errors. 2) The corrected deflection values calculated using the AUTC-CPM method closely align with the FE model deflection values across the entire range of offsets.

This close alignment between the corrected deflection values and the FE model values validates the accuracy of the correction method. By effectively reducing the discrepancies observed in the original TSD measurements, the AUTC-CPM method ensures that the deflection data accurately reflect the actual pavement conditions. Consequently, this approach enhances the reliability and practicality of TSD data for semi-rigid pavement structures, providing a robust basis for precise integration and calculation of deflection values in road engineering applications.

4. Validation of the proposed method for TSD deflection calculation

To verify the accuracy and reliability of the improved deflection calculation method proposed in this paper, a comparative analysis was conducted with existing deflection calculation methods. By calculating the errors between each method and the measured or theoretical values, the accuracy and applicability of different methods were analyzed.

4.1. Validation of accuracy and repeatability in TSD measurements

To evaluate the accuracy and repeatability of TSD device, the pavement deflections measured between 0 and 350 metres within a test section were analyzed. The analysis results were used to represent the impacts of different vehicle speeds on TSD deflection measurements and variations of results from two parallel tests.

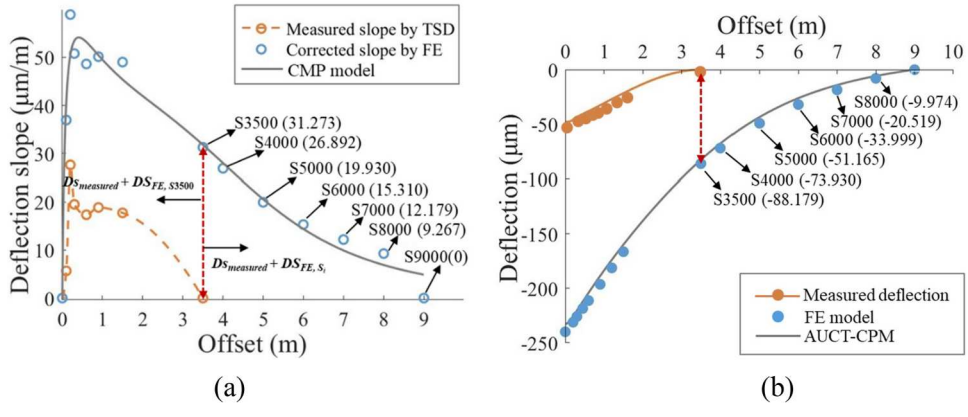

Figure 9. Comparison of the corrected deflection slope and deflection. (a) Measured slope by TSD, corrected slope by FE, CMP model (Data labels in μm/m); (b) Measured deflection, FE model, AUCT-CPM (Data labels in μm).

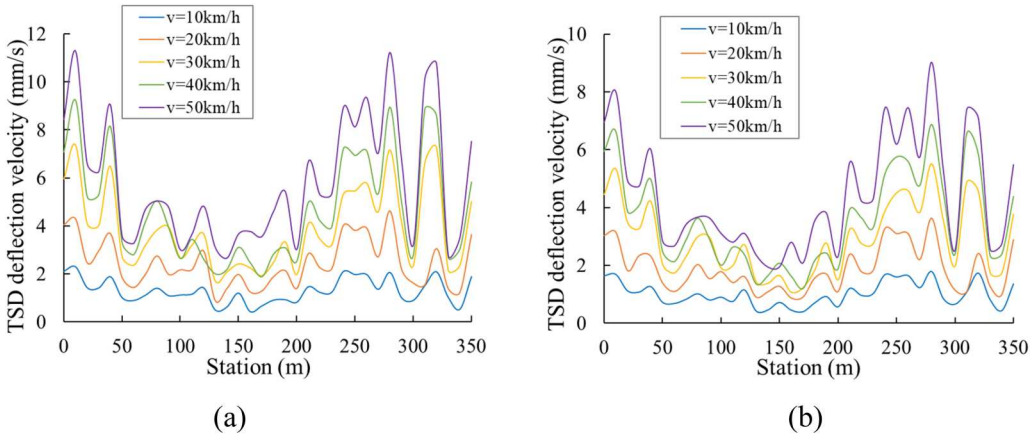

Figure 10. TSD measurements along the longitudinal test section (a) S100; (b) S300.

4.1.1. Impacts of vehicle speeds on TSD deflection measurements

Figure 10 compared the vertical deflection velocity measured at the sensor positions S100 and S300 at different driving speeds.

Figure 10 illustrates the fluctuations in TSD measurement data along different longitudinal stations, reflecting the structural characteristics of the pavement at various locations. The vertical deflection velocities showed consistent trends along the pavement. At the S100 and S300 sensor positions, the driving speed of TSD shows a significant impact on vertical deformation. The peak deflection velocities increase with the rises of speeds, indicating more intense pavement responses at higher speeds. These observations confirm that TSD measurements can accurately capture the visco-elastic responses of asphalt pavements under varying operational conditions. Furthermore, the measured deflections exhibited similar fluctuation patterns at different vehicle speeds, confirming the stability of TSD devices.

4.1.2. Repeatability of measurements

To reveal the stability of TSD measurements, three repeated tests (denoted as TSD-I, TSD-II, and TSD-III) were conducted on the test section at 10 and 30 km/h. The deflection velocities at the sensor position of S100 measured from three repeated tests are compared in Figure 11.

As shown in Figure 11, it is seen that the TSD measurements from three repeated tests show a high consistency, regardless of vehicle speeds. This indicates low variability in the repeated measurements, demonstrating excellent reliability and consistency. These observations demonstrate that TSD measurements reliably capture the viscoelastic responses of pavements. The consistency across different speeds and repeated tests validates the effectiveness of TSD in assessing pavement conditions, thus providing valuable data for maintenance and management decisions.

4.2. Comparison of the proposed method with other deflection calculation methods

The Winkler Foundation Beam Model (WFBM), PCHIP, and the CPM equation proposed in this study were used to fit the measured TSD deflection slope data. Then, by integrating the deflection slopes at various offsets, the deflection values were obtained using different methods. The deflection values calculated by each method were compared with the measured deflection values, which are derived from the Greenwood algorithm. Finally, the *RMSE* was analyzed to compare the calculated and measured deflection values. The relevant results are shown in Figure 12 and Table 4.

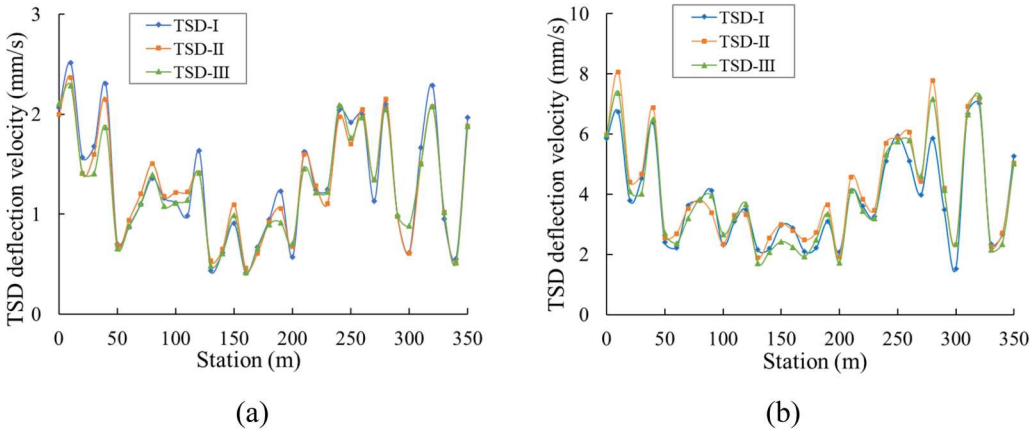

Figure 11. The deflection velocities measured from three repeated tests at: (a) 10 km/h; (b) 30 km/h.

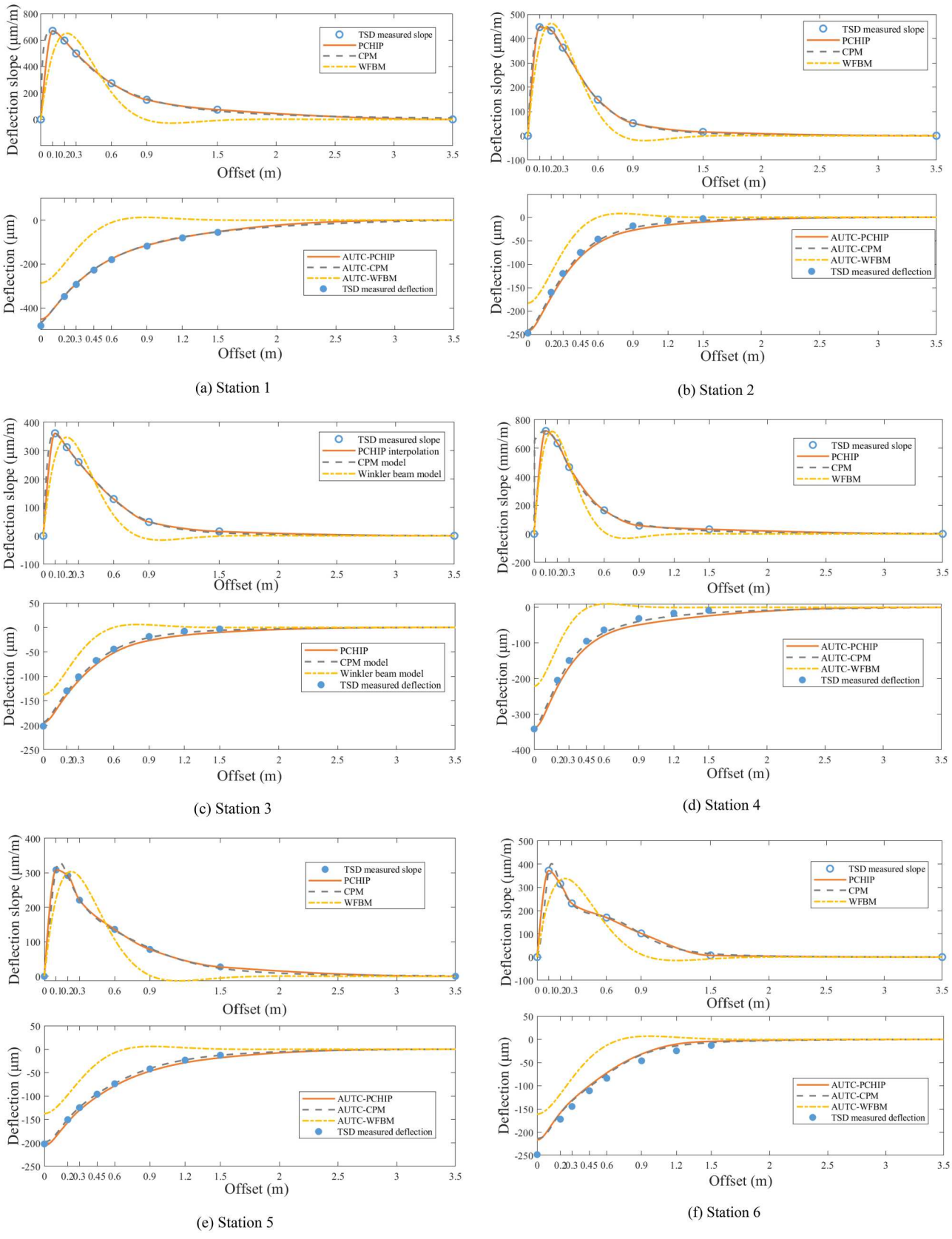

Figure 12. Fitting results of different deflection slopes/deflection compared to measured values.

Figure 12 shows the errors between the deflection values calculated by the three different methods and the actual measured values. It can be seen that the AUTC-PCHIP method and the AUTC-CPM are closer to the TSD measured deflection values, indicating that these two methods better reflect the measured conditions. In contrast, the AUTC-

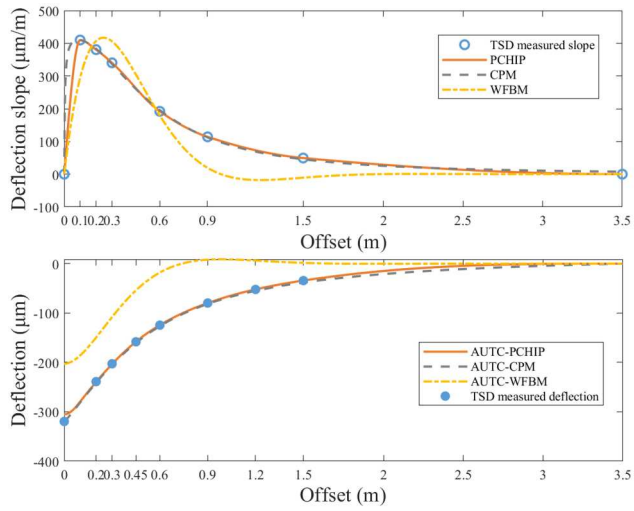

(g) Station 7

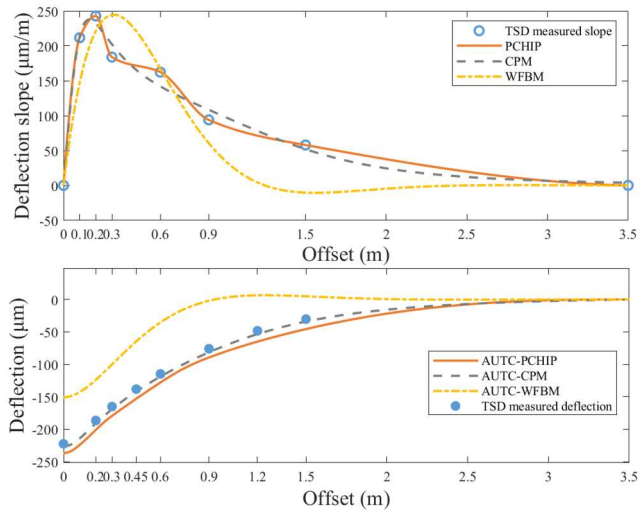

(h) Station 8

Figure 12 *Continued*

WFBM method shows a larger deviation from the measured data.

As shown in Table 4, although the CPM method has lower *RMSE* values in most cases, there are specific instances where the PCHIP method performs comparably (e.g. at Station 7 or Station 9). Therefore, while the CPM method shows promise due to its adaptability to nonlinear data and varying conditions, the performance of the PCHIP method is also noteworthy and cannot be disregarded.

In summary, the selection of a deflection slope model should consider not only the *RMSE* values but also the specific context and conditions of the pavement analysis. Both CPM and PCHIP methods have their respective strengths, and the choice between them should be guided by the particular requirements of the pavement assessment scenario. The CPM provides high adaptability to nonlinear data and its characteristics, enabling the AUTC-CPM method to handle diverse real-world scenarios and maintain high prediction accuracy under different subgrade conditions and load characteristics. Therefore, the AUTC-CPM method has significant advantages in terms of adaptability and flexibility compared to the AUTC-PCHIP method. However, since the measured TSD deflection slopes are corrected values based on sensor S3500,the current use of measured values serves primarily to evaluate the reasonableness of the curve shapes rather than their absolute accuracy. It is necessary to use other methods to further verify the accuracy of the fitting model.

Table 4. The RMSE of deflection compared to measured deflection values.

RMSE (μm)	Station 1	Station 2	Station 3	Station 4
AUTC-PCHIP	10.9739	8.6898	7.7112	16.4821
AUTC-CPM	6.6201	4.4197	3.8348	7.8892
AUTC-WFBM	145.9476	41.0317	40.2624	77.3731
RMSE (μm)	Station 5	Station 6	Station 7	Station 8
AUTC-PCHIP	4.9645	17.2013	5.1264	14.6032
AUTC-CPM	1.8198	2.5515	2.3942	4.3613
AUTC-WFBM	52.7629	88.2024	90.3166	65.889

4.3. Comparison of the proposed method with the theoretical values by FE method

To further verify the accuracy of the improved deflection calculation method, this study intends to use theoretical values obtained by the FE method as a benchmark. The deflection values obtained from the AUTC-PCHIP method and the proposed corrected deflection calculation method will be compared, and the errors between these methods and the theoretical deflection values calculated by the FE method will be computed. The specific comparison scheme is as follows:

1) Use the deflection slopes of the semi-rigid pavement structure obtained from FE model. Read the values at offsets S100, S200, S300, S600, S900, S1500, and S3500. Use the reading at S3500 as the baseline, subtracting the S3500 reading from the readings at these offsets to simulate the TSD vehicle's test values. Then, use the AUTC-PCHIP method to obtain the fitted deflection curve.
2) Directly read the values at the above offsets, setting the zero-position of the deflection slope at 9,000 mm from the load centre. Then, use the AUTC-CPM method to obtain the fitted deflection curve.
3) Calculate the *RMSE* between the fitting results of each method and the theoretical deflection values obtained from the FE model. The relevant results are shown in Figure 13 and Table 5.

Figure 13 shows that selecting the offset of the reference sensor (i.e. the position where the theoretical deflection slope is 0 μm/m) and the form of the deflection slope curve are crucial for accurately determining the deflection of semi-rigid pavements. 1) Integration starting position: the position where the deflection slope of the semi-rigid asphalt pavement is set to zero determines the starting position for integration.

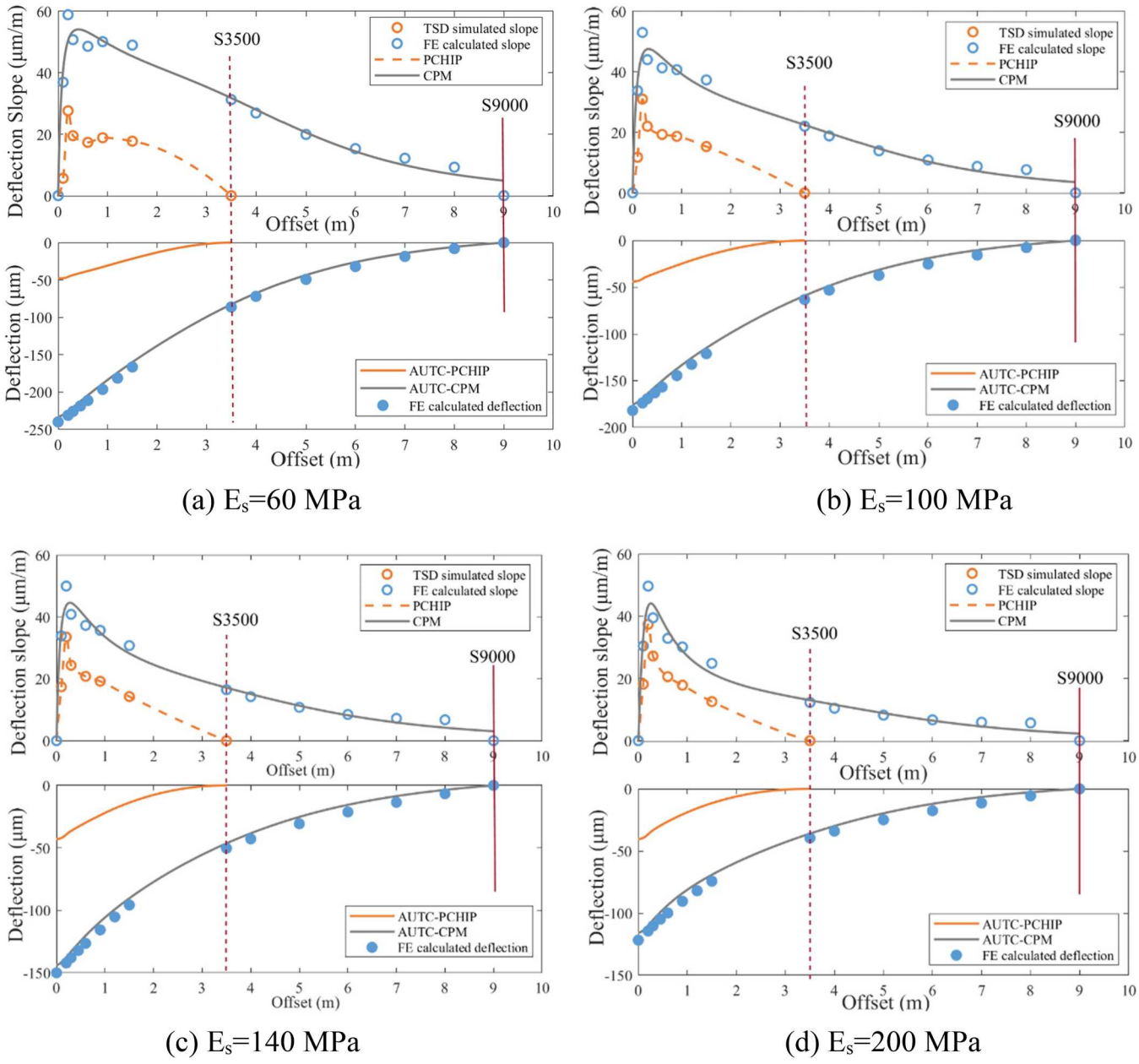

Figure 13. Comparison of different deflection slope curves with theoretical values.

This starting position significantly affects the shape of the surface deflection basin. Choosing the starting position at S3500 or S9000 results in different deflection basin shapes due to the shifting of the measurement baseline. An inappropriate starting position can lead to inaccurate descriptions of pavement response, particularly near the load centre. 2) Curve form: the form of the deflection slope curve obtained through PCHIP or the CPM determines the smoothness of the curve transition and fit with actual pavement behaviour. PCHIP can ensure a smooth transition of the overall data trend, but its suitability for reflecting the true deflection slope profile of the pavement is uncertain. On the other hand, the CPM provides a more accurate representation of the nonlinear characteristics of pavement deflection slopes.

Furthermore, as shown in Table 5, the AUTC-CPM method displays lower *RMSE* values compared to the AUTC-PCHIP method across different test scenarios when compared to the deflection values calculated by the FE method. This indicates that the AUTC-CPM method has higher accuracy and is better able to capture the complex behaviour of semi-rigid pavements under load. This superiority arises from the AUTC-CPM method's ability to adapt to a wider range of deflection shapes and its higher sensitivity to different pavement conditions.

Therefore, the reasonable selection of the integration starting position and curve form has a profound impact on accurately predicting pavement deflection. The improved deflection calculation method can effectively enhance the

Table 5. The RMSE of deflection compared to the deflection by FE model.

RMSE (μm)	E_s = 60MPa	E_s = 100 MPa	E_s = 140MPa	E_s = 200MPa
AUTC-PCHIP	165.0529	118.7782	92.4369	70.3091
AUTC-CMP	5.8267	5.7993	5.3294	5.1707

accuracy and scientific validity of TSD measured values, thereby providing stronger technical support for the design, maintenance, and management of road engineering.

5. Conclusions and discussions

This study aims to develop an improved deflection calculation method using curve area integration, enabling more accurate and rapid calculation of deflection basins under TSD loads. The main findings of the study are summarised as follows:

(1) FE simulations were conducted to evaluate the deflection responses of asphalt pavements under TSD loads. The effects of various factors, such as vehicle speed, layer modulus, and structural thickness, on TSD deflections were assessed. The results showed that the deflection slope characteristics and extremum features of flexible pavements differ significantly from those of semi-rigid pavements. Due to their distinct viscoelastic properties, semi-rigid pavements exhibit slower deflection responses, highlighting the necessity for precise deflection slope calibration in TSD assessments to prevent errors in pavement evaluations.

(2) TSD deflection slopes were corrected using semi-rigid pavement structures as an example. For sensor offsets ≤ 3,500 mm, a fixed value from the FE model at 3,500 mm was uniformly applied. For offsets > 3,500 mm, the values derived from the FE model were directly added. This method ensures that data at each sensor offset accurately reflect pavement conditions and facilitates the subsequent integration calculation of deflection values, improving the reliability and practicality of TSD measurements for semi-rigid pavements.

(3) By varying the subgrade modulus, the rate of change of the deflection slope at each offset was calculated, and the actual range of load propagation on semi-rigid pavements was determined. This allowed for the establishment of a more scientific reference baseline. The results showed that as the distance increased, the rate of change of the deflection slope gradually decreased and stabilised at 9,000 mm. Therefore, the reference sensor should be positioned at least 9,000 mm from the load centre to ensure the accuracy of TSD deflection calculations and the reliability of the data.

(4) Multiple models were selected to fit the deflection slope data under different pavement conditions and loading conditions. By calculating and comparing the R^2 and *RMSE* associated with different curve forms, the Composite Polynomial Model (CPM) was identified as providing the optimal fitting accuracy.

(5) Through comparative analysis with the AUTC-WFBM and AUTC-PCHIP method, it was verified that the deflection calculated using the AUTC-CPM method in this study was closer to the measured values and values obtained by the FE model. This indicates that the AUTC-CPM method not only more accurately reflects pavement deflection behaviour under actual loading conditions but also has higher accuracy in capturing the complex behaviour of semi-rigid pavements under load.

In the study presented, deflection and slope calculations are improved through the incorporation of FE modelling and viscoelastic property corrections, offering a more reliable assessment of asphalt pavement conditions. Nevertheless, it is acknowledged that certain limitations remain. Critical factors such as pavement roughness and the variability in asphalt mixtures were not exhaustively addressed, yet these are essential for comprehensively understanding pavement behaviour under TSD loads. Moreover, the correction method proposed has not yet been validated against other deflection measurement techniques. It is imperative for future research to broaden the scope of asphalt mixtures examined and to assess the impact of pavement roughness on TSD measurements more thoroughly. Validating the proposed method across diverse field conditions and against various deflection measurement techniques is necessary to ensure the robustness and applicability of the findings. These steps are crucial for advancing our understanding and application of the method in practical scenarios.

Disclosure statement

No potential conflict of interest was reported by the author(s).

Funding

This work was supported by National Natural Science Foundation of China: [grant number 52272323]; Enterprise Innovation Development and Energy Level Enhancement Project of Shanghai State owned Assets Supervision and Administration Commission: [grant number 2024016]; Key Engineering Science and Technology Project of Jiangxi Provincial Department of Transportation: [grant number 2024ZG006]; Hebei Provincial Department of Transportation's Science and Technology: [grant number JX-202001]; Research Project of Anhui Transportation Holdings Group: [grant number JKKJ-2023-12].

References

Andren, P., and Lenngren, C.A., 2000. Evaluating pavement layer properties with a high-speed rolling deflectometer. *Proceedings of SPIE - The International Society for Optical Engineering*, doi:10.1117/12.385026.

Austroads, 2016. Pavement data collection with a traffic speed deflectometer (TSD) device, Austroads Test Method, AGAM-T017-16.

Beizaei, M., 2023. An approach for verification of traffic speed deflectometer measurements, (Order No. 30486933), *The University of Texas at El Paso ProQuest Dissertations & Theses*, 2023. 30486933.

Březina, I., Stryk, J., and Grošek, J., 2017. Using traffic speed deflectometer to measure deflections and evaluate bearing capacity of asphalt road pavements at network level. *IOP Conference Series: Materials Science and Engineering*, 236, 012102. doi:10.1088/1757-899X/236/1/012102.

Cao, D., *et al.*, 2019. Comparisons of asphalt pavement responses computed using layer properties backcalculated from dynamic and static approaches. *Road Materials and Pavement Design*, 20, 1114–1130. doi:10.1080/14680629.2018.1436467.

Chen, Z., *et al.*, 2024. Conversions of viscoelastic deflections of asphalt pavement under TSD load to elastic ones for pavement condition assessments. *Road Materials and Pavement Design*, 10, 1–23. doi:10.1080/14680629.2024.2338780.

Cheng, H., *et al.*, 2021. Relationships between asphalt-layer moduli under vehicular loading and FWD loading. *Journal of Materials in Civil Engineering*, 33, 04020437. doi:10.1061/(ASCE)MT.1943-5533.000342.

Cheng, H., Liu, L., and Sun, L., 2019. Determination of layer modulus master curve for steel deck pavement using field-measured strain data. *Transportation Research Record*, 2673, 617–627. doi:10.1177/0361198119828685.

Cheng, H., Liu, L., Sun, L., *et al.*, 2020. Comparative analysis of strain-pulse-based loading frequencies for three types of asphalt pavements via field tests with moving truck axle loading. *Construction and Building Materials*, 247, 118519. doi:10.1016/j.conbuildmat.2020.118519.

Deng, Y., 2017. *Three-dimensional numerical simulation of pavements deflection basins under moving loads*. Texas: Texas A&M University.

Deng, Y., *et al.*, 2019. 3D simulation of deflection basin of pavements under high-speed moving loads. *Construction and Building Materials*, 226, 868–878. doi:10.1016/j.conbuildmat.2019.07.228.

Duschlbauer, D., and Lee, J. 2021. Capturing the moving deflection basin under a traffic speed deflectometer. In: Z. Hossain, M. Zaman, and J. Zhang, eds. *Finding solutions of the 21st century transportation problems through research and innovations*, China: Springer, 23–33.

Fan, J., *et al.*, 2022. Characteristics of high-speed deflection basin and structural parameter back-calculation of asphalt pavement with different structural states. *Construction and Building Materials*, 341, 127869. doi:10.1016/j.conbuildmat.2022.127869.

Federal Highway Administration, 2016. *Pavement structural evaluation at the network level, FHWA-HRT-15-074*. Washington, DC: United States. Department of Transportation. Federal Highway Administration. Office of Infrastructure Research and Development.

Graczyk, M., *et al.*, 2014. Analytical solution of pavement deflections and its application to the TSD measurements. *In*: *26th arrb conference, ARRB, Sydney*.

Greenwood Engineering, 2022. Traffic speed deflectometer, Brondby, Denmark. https://greenwood.dk/road/tsd/ (accessed 24 July 2024).

Hu, Y., Cheng, H., and Sun, L., 2022. Vertical compressive strain-based method for setting the rigid layer depth based on falling weight deflectometer test. *Construction and Building Materials*, 319,, 126156. doi:10.1016/j.conbuildmat.2021.126156.

Huang, B., *et al.*, 2022. Evaluation of traffic speed deflectometer for collecting network level pavement structural data in Tennessee (No. RES2020-08), Tennessee Department of Transportation.

Jia, X., *et al.*, 2021. Evaluation of influence of pavement data on measurement of deflection on asphalt surfaced pavements utilizing traffic speed deflection device. *Construction and Building Materials*, 270, 121842. doi:10.1016/j.conbuildmat.2020.121842.

Krarup, J., *et al.*, 2006. Output from the greenwood traffic speed deflectometer. In: *22nd arrb conference: research into practice, Canberra, Australia, 29 October - 2 November*, 1–10.

Lee, J., Moffatt, M., and Ramanujam, J.M., 2016. Exploratory study to use traffic speed deflectometers (TSD) for project-level pavement evaluations. *Geo-China*, 2016, 1–8. doi:10.1061/9780784480090.001.

Mabrouk, G.M., *et al.*, 2022. 3D-finite element pavement structural model for use with traffic speed deflectometers. *International Journal of Pavement Engineering*, 23, 4065–4079. doi:10.1080/10298436.2021.1932880.

Madsen, S.S., and Pedersen, N.L., 2022. Comparison of RAPTOR measurements with falling weight deflectometer deflections using backcalculation. In: I. Huff, H. Merk, and R.G. Saba, eds. *Eleventh international conference on the bearing capacity of roads, railways and airfields*, 33–44. Boca Raton: CRC Press.

Manoharan, S., Chai, G., and Chowdhury, S., 2020. Structural capacity assessment of Queensland roads using traffic speed deflectometer data. *Australian Journal of Civil Engineering*, 18, 219–230. doi:10.1080/14488353.2020.1766301.

Ministry of Transport of the People's Republic of China, 2017. Specifications for design of highway asphalt pavement (JTG D50-2017), China Communications Press, Beijing, People's Republic of China. [In Chinese].

Muller, W.B., and Roberts, J., 2013. Revised approach to assessing traffic speed deflectometer data and field validation of deflection bowl predictions. *International Journal of Pavement Engineering*, 14, 388–402. doi:10.1080/10298436.2012.715646.

Nam, B.H., 2011. Transition of the rolling dynamic deflectometer device from a screening tool to an evaluation tool for rigid airfield pavement projects. *Transportation Research Record*, 2206, 39–51. doi:10.3141/2206-06.

NCHRP 1-37A Final Report, 2004. *Guide for mechanistic-empirical design of new and rehabilitated pavement structures*. Washington, D.C.: Transportation Research Board.

Park, S.W., and Schapery, R., 1999. Methods of interconversion between linear viscoelastic material functions. Part I-A numerical method based on Prony series. *Journal of Solids and Structures*, 36 (11), 1653–1675. doi:10.1016/S0020-7683(98)00055-9.

Pedersen, L., 2013. *Viscoelastic modelling of road deflections for use with the traffic speed deflectometer*. Lyngby: Technical University of Denmark.

Rasmussen, S., Susanne, L.A., and Jorgen, B., 2008. *A comparison of two years of network level measurements with the traffic speed deflectometer*. Ljubljana: Transport Research Arena Europe.

Roussel, J.M., *et al.*, 2019. Numerical simulation of falling/heavy weight deflectometer test considering linear viscoelastic behaviour in bituminous layers and inertia effects. *Road Materials and Pavement Design*, 20, S64–S78. doi:10.1080/14680629.2019.1587491.

Roussel, J.M., *et al.*, 2022. Influence of interface properties on heavy weight deflectometer test results. *Road Materials and Pavement Design*, 23, 162–177. doi:10.1080/14680629.2022.2029759.

Shen, K., and Wang, H., 2023. Impact of dynamic loading on pavement deflection measurements from traffic speed deflectometer. *Measurement*, 217, 113086. doi:10.1016/j.measurement.2023.113086.

Shi, Z., *et al.*, 2022. Peridynamics for fracture analysis of reflective cracks in semi-rigid base asphalt pavement. *Applied Sciences*, 12, 3486. doi:10.3390/app12073486.

Steele, D., *et al.*, 2019. Development of a high speed rolling wheel deflectometer, 88th Transportation Research Board Annual Meeting, Washington, DC.

Steele, D., Lee, H., and Beckemeyer, C.A., 2020. Development of the rolling wheel deflectometer (RWD), No. FHWA-DTFH-61-14-H00019, United States Federal Highway Administration.

Steiner, D., *et al.*, 2016. Impact of loading rate and temperature on tensile strength of asphalt mixtures at low temperatures. In: *8th rilem international conference on mechanisms of cracking and debonding in pavements, springer Netherlands*, 69–74.

Sun, Z., *et al.*, 2023. A parameter identification technique for traffic speed deflectometer tests of pavements. *Road Materials and Pavement Design*, 24, 1065–1087. doi:10.1080/14680629.2022.2060125.

Wu, C., *et al.*, 2020. Asphalt pavement modulus backcalculation using surface deflections under moving loads. *Computer-Aided Civil and Infrastructure Engineering*, 35, 1246–1260. doi:10.1111/mice.12624.

Xiao, F., *et al.*, 2021. Utilization of traffic speed deflectometer for pavement structural evaluations. *Measurement*, 178, 109326. doi:10.1016/j.measurement.2021.109326.

Zhang, M., *et al.*, 2023. Huang, relationship between fatigue condition of asphalt pavements and deflection lag from traffic speed deflectometer. *Journal of Materials in Civil Engineering*, 35, 04023186. doi:10.1061/JMCEE7.MTENG-15329.

Zhang, B., *et al.*, 2024. Mechanical analysis of semi-rigid base asphalt pavement under the influence of groundwater with the spectral element method. *Applied Sciences*, 14, 2375. doi:10.3390/app14062375.

Zofka, A., *et al.*, 2014. Alternative approach for interpreting traffic speed deflectometer results. *Transportation Research Record*, 2457, 12–18. doi:10.3141/2457-02.

Appendix

Using Table Curve software, nine curve forms of TSD deflection basins were initially selected, as detailed in Eq. (A.1) through Eq. (A.9).

Third-order CPM Equation:

$$y = \frac{a + cx + ex^2 + gx^3}{1 + bx + dx^2 + fx^3} \tag{A.1}$$

Second-order CPM Equation 2/2:

$$y = \frac{a + cx + ex^2}{1 + bx + dx^2} \tag{A.2}$$

Second-order CPM Equation1/2:

$$y = \frac{a + cx}{1 + bx + dx^2} \tag{A.3}$$

Second-order CPM Equation 0/2:

$$y = \frac{a}{1 + bx + cx^2} \tag{A.4}$$

Composite rational Equation

$$y = \frac{1}{a + bx + ce^x} \tag{A.5}$$

Cubic rational Equation:

$$y = \frac{1}{a + bx + cx^2 + dx^3} \tag{A.6}$$

Quadratic rational Equation:

$$y = \frac{1}{a + bx + cx^2} \tag{A.7}$$

Quintic polynomial Equation:

$$y = a + bx + cx^2 + dx^3 + ex^4 + fx^5 \tag{A.8}$$

Quartic polynomial Equation:

$$y = a + bx + cx^2 + dx^3 + ex^4 \tag{A.9}$$